THE JOURNAL OF PHYSICAL CHEMISTRY B

Article

pubs.acs.org/JPCB

Molecular Dynamic Studies of Transportan Interacting with a DPPC Lipid Bilayer

Mohsen Pourmousa,[†] Jirasak Wong-ekkabut,[‡] Michael Patra,[§] and Mikko Karttunen*[,∥]

[†]Department of Applied Mathematics, The University of Western Ontario, London, Ontario, Canada N6A 5B7

[‡]Department of Physics Faculty of Science, Kasetsart University, 50 Phahon Yothin Road, Chatuchak Bangkok 10900, Thailand

[§]Department of Physical Chemistry, Lund University, Sweden

[∥]Department of Chemistry, University of Waterloo, 200 University Avenue West, Waterloo (ON), Canada N2L 3G1

ABSTRACT: Translocation of peptides through cellular membranes is a fundamental problem in developing antimicrobial peptides and in drug delivery. There is a class of peptides, known as cell-penetrating peptides, that are able to penetrate membranes without disrupting them. They can carry pharmacological compounds, thus a promising strategy for drug delivery. The physical mechanisms that facilitate translocation are not known. We have used large-scale molecular dynamics simulations to study the penetration of transportan across a zwitterionic dipalmitoyl-phosphatidyl-choline (DPPC) bilayer. We obtained the free energy profile for one peptide inside the bilayer and discuss the response of the bilayer to the presence of transportan. We also discuss the importance of lysine residues and speculate on the possible penetration mechanism of the peptide and propose a graded-like penetration process.

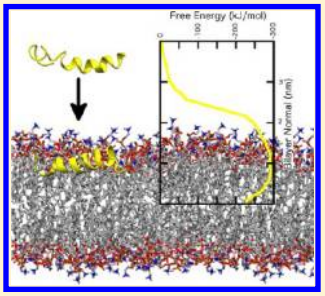

INTRODUCTION

Cell-penetrating peptides (CPPs) are short peptides of less than 30 amino acids that are able to penetrate cell membranes and transport different cargoes into cells without disrupting them.[1] Most of these peptides have a positive net charge and/or an amphipathic nature but can otherwise have very different characteristics.[2] The physical mechanisms of translocation are not known, and current knowledge is more empirical than predictive. Because different amino acid motifs have been observed in different CPPs, it is believed that the translocation mechanisms differ for different CPPs.[1] A hypothesis is that kinetics of penetration, rather than the peptide's sequence, is important in translocation mechanism, and the sequence matters indirectly.[3]

In general, the mechanism of penetration seems to be receptor and energy independent.[1] In certain cases, translocation can be partially mediated by endocytosis.[4,5] A variety of possible mechanisms have been proposed for CPPs and AMPs. These include the carpet model,[6] the barrel-stave model,[7] the toroidal-pore model,[8] the sinking-raft model,[9] the formation of inverted micelles,[10] local electroporation,[11] micropinocytosis,[12] and direct insertion of an unfolded peptide into the membrane.[13]

Cargoes that are successfully translocated by CPPs range from small molecules, such as small peptides or fluorescent labels, to proteins and supermolecular particles.[1] Most CPPs are inert or have insignificant side effects.[1] The half-time of penetration of these peptides ranges from 3 to 20 min.[1] CPPs are novel vehicles for delivering cargoes into cells and have promising applications in drug delivery.

Transportan (GWTLN SAGYL LGKIN LKALA ALAKK IL-amide), a 27 amino-acid-long member of a class of galanin-based chimeric peptides, is one of the amphipathic cell-penetrating peptides designed and synthesized in 1996.[14] It consists of 12 N-terminal residues of galanin, 14 C-terminal residues of mastoparan, and a connecting lysine. Galanin is a neuropeptide that is widely expressed in the brain, spinal cord, and gut of mammals,[15] and mastoparan is a peptide toxin from wasp venom.[16] Transportan is an amphipathic peptide having distinct hydrophobic and hydrophilic residues. There are also other versions of transportan,[17,18] e.g., transportan-10, all of which show penetration to some extent. The studies using the transportan family have made it a representative member of amphipathic CPPs.

Several experiments have been performed on transportan/lipid systems,[19−23] but the penetration mechanism has remained unknown. It has been shown[21] that internalization of radiolabeled transportan is receptor/protein independent. The peptide penetrates into every mammalian cell type (Bowes's melanoma, HeLa, HEK293, Jurkat, etc.) with the same localization on the plasma membrane, nuclear membrane, and all other intracellular membrane structures. In the same study, it was shown that receptor-mediated endocytosis cannot be involved in the cellular uptake of the peptide, since penetration is not blocked by the presence of inhibitors of endocytosis. Penetration was observed to be slightly concentration dependent with a higher relative uptake at lower concentrations (5 nM) compared to higher concentrations (500 nM).[21] Transportan has close to random coil secondary structure in water[22] but adopts a helical structure when bound to phospholipid bicelles as well as SDS micelles with the helix mostly localized to the mastoparan part.[22]

Received: April 16, 2012
Revised: December 5, 2012
Published: December 6, 2012

Atomistic molecular dynamics (MD) simulations have been performed on CPPs and AMPs.[12,17,24−27] In some[25−27] but not all, translocation was observed within simulation times (hundreds of nanoseconds). Spontaneous pore formation was not observed for penetratin (a CPP) interacting with phospholipids such as palmitoyl-oleoyl-phosphatidyl-choline (POPC), palmitoyl-oleoyl-phosphatidyl-glycerol (POPG), palmitoyl-oleyl-phosphatidic-acid (POPA), and palmitoyl-oleoyl-phosphatidyl-serine (POPS) membranes,[24] and for the 21-amino-acid-long transportan analogue, transportan-10 (a CPP), interacting with POPC,[17] and for penetratin and TAT peptide (a CPP which is obtained from the transcription transactivation protein from human HIV-1 virus) with dioleoyl-phosphatidyl-choline (DOPC) and dipalmitoyl-phosphatidyl-choline (DPPC) membranes.[12] Penetration was observed, however, for melittin (an AMP) interacting with DPPC membranes,[25] magainin-2 (an AMP) with DPPC membranes,[26] and also TAT peptide with DOPC membranes,[27] although the latter simulation has been argued not to represent experimental conditions appropriately,[12] as their system was strongly charged and not neutralized by counterions leading to a high membrane expansion.[27]

Most of the experimental studies of peptide−membrane systems have the disadvantage of using perturbative probes attached to peptides. Computer simulations are helpful in gaining detailed information about biophysical systems and can be regarded as complementary to experiments. The spontaneous translocation of CPPs is known to be a rare process,[1] making it very hard to simulate translocation within currently accessible simulation times. However, simulating these peptides can shed light on the possible translocation mechanism in that, by studying the peptide/membrane interactions and behavior, some mechanisms can be ruled out or the peptide/membrane behaviors can be studied in early stages of penetration. This task is highly demanding for the case of transportan whose mode of action is not well understood. Questions such as the significance of some residues, the free energy barrier in the translocation process, and the response of the membrane to the presence of transportan can be addressed by MD simulations. Understanding the detailed behavior of CPPs and AMPs would enable the development of designer peptides based on these properties. To our knowledge, no computer simulation has been reported on transportan interacting with a bilayer. We present results of atomistic MD simulations performed in an attempt to better understand the nature of interaction between transportan and a zwitterionic membrane, namely, DPPC.

The rest of the article is comprised of four sections: Simulation Details, Analysis, Results and Discussion, and Conclusion. In the section Simulation Details, the simulation protocol will be presented. In the section Analysis, the details of the analysis methods will be presented. In the section Results and Discussion, the results of three sets of simulations, including simulations of transportan starting from the water phase, simulations of transportan starting from the bilayer core, and simulations related to the free energy calculations, will be provided and discussed. We finish with a summary of the results in the Conclusion section.

SIMULATION DETAILS

Translocation of CPPs is difficult to capture with the current accessible time scales of MD simulations. We chose two strategies to overcome this obstacle: First, we placed the peptide initially in the water phase and let it interact with the bilayer. Second, we placed the peptide inside the bilayer core to study the spontaneous response of the bilayer to the peptide. Moreover, by restraining the peptide at different depths of the bilayer, we computed the free energy profile of the system. In addition to the above sets of simulations which all consisted of a single peptide interacting with the bilayer, we simulated the interaction of multiple peptides with the bilayer corresponding to a peptide/lipid ratio of 2/128, 3/128, 4/128, and 5/128. In none of the multiple-peptide simulations was the penetration of the peptides more than the one in simulations of a single peptide. The mode of penetration was always observed to be the same. Therefore, we focus on the case of a single transportan peptide interacting with a bilayer.

All simulations were performed at constant temperature and pressure with a constant number of particles (NpT ensemble). Simulations were done using Gromacs 4.0.5.[28] The simulated systems consisted of 2 × 64 DPPC lipids hydrated with ∼7500 water molecules and one transportan peptide. The initial size of the system was 6.5 × 6.5 × 9.5 nm^3. Figure 1 shows the atom numbering of DPPC and the helical wheel diagram of the peptide.

For lipids, we used the coordinates of a previous 100 ns simulation of DPPC lipids in water[29] to which we added transportan. The initial conformation of transportan was obtained from a nuclear magnetic resonance (NMR) study of transportan interacting with phospholipid bicelles (PDB code: 1SMZ).[19] The four positive charges of transportan were

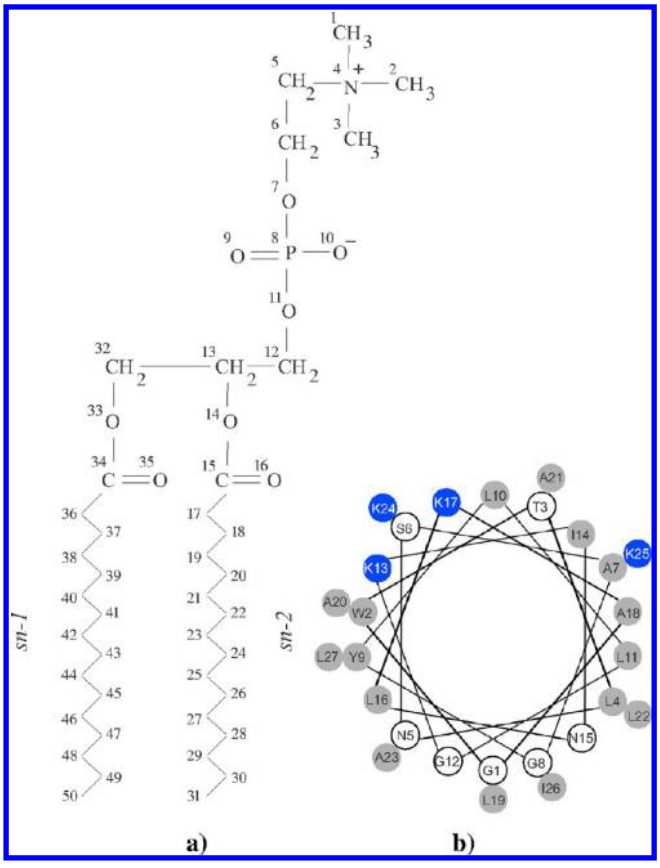

Figure 1. (a) Schematic representation of DPPC. (b) The helical wheel diagram of transportan (GWTLN SAGYL LGKIN LKALA ALAKK IL-amide). Each residue is categorized according to the following color scheme: *white* (hydrophilic), *gray* (hydrophobic), and *blue* (charged).

dx.doi.org/10.1021/jp310255r | J. Phys. Chem. B 2013, 117, 230−241

compensated for by the corresponding number of Cl^- counterions to ensure charge neutrality. The systems were energy minimized using the steepest descent method, which is implemented in Gromacs, before MD simulations. Eight simulations were run to ~90 ns, one to 320 ns, and one to 780 ns.

DPPC was modeled with the Berger et al. parametrization,[30] and the GROMOS force field[31,32] was used for transportan. In general, GROMOS and its various revisions have been shown to work well with lipids, in particular DPPC, and proteins.[33,34] There also have been some revisions to the Berger parametrization,[35−37] but we chose to use the original Berger forcefield together with the GROMOS87, as this combination has been widely used and well tested by several groups.[12,17,24,27] Water was modeled with the simple point charge model (SPC).[38] The temperature was kept constant at 323 K using the Berendsen weak coupling algorithm.[39] It also speeds up the dynamics of the system in view of the slowness of translocation of the peptide. As in all simulations of this type, the heat bath of lipids and the peptide was separated from the heat bath of the solution to produce a homogeneous temperature in the entire system and avoid any possible artifacts. Both heat baths had a coupling constant of 0.1 ps. The pressure was kept at 1 bar using the Berendsen algorithm[39] with a time constant of 0.1 ps. Pressure was applied semi-isotropically, i.e., the extension of the simulation box in the bilayer normal direction (z) and its cross-section area in the bilayer plane (xy) could vary independently. The Lennard-Jones and the real-space parts of electrostatic interactions were cut off at 1.0 nm. The particle mesh Ewald (PME) method[40] was used to compute long-range interactions; it has been shown that the truncated electrostatic methods lead to physical artifacts in bilayer systems.[29,41] All bonds and angles were constrained to their equilibrium values using the linear constraint solver (LINCS) algorithm.[42] The time step for all simulations was set to 2 fs. The above protocol was applied throughout the entire study.

The umbrella sampling (US) method[43] was used to compute the potential of mean force (PMF). In the US method, the free energy is obtained from a set of equilibrated simulations. An external potential, or a biasing potential, acts on the center of mass (COM) of a chosen group of atoms to restrain a certain degree of freedom of the group and the rest of the molecule remains unconstrained. Here, at each step which we refer to as a window, the peptide was restrained at a certain distance from the bilayer. A biasing harmonic potential with a force constant of 3000 kJ mol^{-1} nm^{-2} was used to restrain the peptide in each window. In any two successive windows, the distance between the peptide and the bilayer was changed by 0.1 nm. A total of 41 simulation windows were used to compute the PMF as a function of the peptide−bilayer distance varying from z = 0 nm (bilayer center) to z = 4 nm. The PMF was then calculated from the probability distribution of the peptide when restrained in biased simulations. The weighted histogram analysis method (WHAM)[44] with a relative tolerance of 10^{-11} was used to combine the results from all the windows and produce the free energy profile.

The starting configuration for each window was chosen as follows: For the first 11 windows, corresponding to distances from z = 0.0 nm to z = 1.0 nm, the peptide was pulled from the bilayer center. The initial orientation of the peptide was parallel to the membrane plane. The reason why we pulled the peptide from the bilayer center, and not from the water, was to avoid possible sticking of the peptide to any of the charged head groups which were about 2 nm away from the bilayer center. For other windows, since we already had a 780 ns unbiased simulation, in which the peptide penetrated up to 1.5 nm away from the center of the bilayer, we could extract plausible configurations of the peptide at different distances from the bilayer. We picked those configurations as the starting points for the rest of the windows. Each window was equilibrated for 60 ns, and the production simulations were run for 40 ns. To ensure and test that the chosen simulation times were long enough, we extended the simulations in some of the windows for an additional 50 ns. No changes in the free energy profile were observed.

■ ANALYSIS

We are primarily interested in local properties, i.e., the lipids that are neighboring the peptide. To define a neighborhood, we use a circle on the xy plane with radius d to the center of any component of the peptide. Lipids are defined as interacting with transportan if any component of them lies within any of the circles. The value of d was selected on the basis of the lateral radial distribution function (RDF) of the peptide with respect to the DPPC atoms. The first minimum of the RDF occurs at ~0.6 nm. Therefore, d was selected to be 0.6 nm. To determine if a hydrogen bond exists, the following criterion was used:[45−47] $r_{HB} < 0.35$ nm and $\alpha < 30°$. The value of 0.35 nm corresponds to the first minimum of the RDF of water. In our system, the −NH and −OH groups of the peptide's backbone are able to form hydrogen bonds with phosphate, glycerol, or carbonyl groups of lipids. For the calculation of order parameter, the numbering shown in Figure 1a was used. Finally, to understand the effect of the presence of transportan on the lipid bilayer, we compared our results with those from a previous 100 ns simulation of a pure DPPC bilayer.[48]

■ RESULTS AND DISCUSSION

The results are presented in three main sections. In the section Equilibrium Simulations 1: Peptide Initially in Solution, the results from equilibrium simulations will be provided. In these simulations, the initial configuration of the system is the one with the peptide in water. The peptide then associates with the bilayer, and its interaction with the bilayer will be investigated. In the section Equilibrium Simulations 2: Transportan Inserted into the Bilayer, the initial configuration of the system is the one with the peptide in the bilayer interior. In the section Simulations 3: Free Energy Calculations, the results of the simulations with a biasing force will be provided. The aim of this section is to find the free energy of the system.

Equilibrium Simulations 1: Peptide Initially in Solution. We performed 10 independent simulations. In all except simulations #3 and #9, the initial configuration of the peptide was parallel to the membrane surface and the peptide was slightly rotated around its helical axis. In the other two simulations, the peptide had an angle less than 90° to the membrane surface. The center of mass (COM) of the peptide was initially placed ~2 nm away from the bilayer surface. Although it did not take more than 10 ns for the peptide to associate with the bilayer, the association was not immediate and the peptide had enough time to randomly move in water before reaching the bilayer. This implies the insensitivity of the results to the peptide's initial configuration when it is far enough from the bilayer surface. Table 1 lists all simulations, their time lengths, and the insertion depth of the peptide. The

Table 1. Details of Different Simulations[a]

number	simulation length (ns)	first approaching terminus	insertion depth
1	86	C-terminus	0.0 ± 0.1 nm (70–86 ns)
2	780	N-terminus	0.5 ± 0.1 nm (700–780 ns)
3	320	C-terminus	0.5 ± 0.1 nm (220–320 ns)
4	90	N-terminus	0.6 ± 0.1 nm (80–90 ns)
5	90	N-terminus	0.4 ± 0.1 nm (80–90 ns)
6	90	C-terminus	0.4 ± 0.1 nm (80–90 ns)
7	90	N-terminus	0.1 ± 0.1 nm (80–90 ns)
8	90	C-terminus	0.5 ± 0.1 nm (80–90 ns)
9	90	C-terminus	0.2 ± 0.1 nm (80–90 ns)
10	90	N-terminus	0.7 ± 0.1 nm (80–90 ns)

[a]The insertion depth is the average distance between the COM of nitrogen atoms and the COM of peptide. The average was taken in the time intervals as indicated.

insertion depth is defined as the distance between the COM of nitrogen atoms of lipids and the COM of the peptide. The longest simulation (780 ns) was used for all major analyses. At $t \sim 780$ ns, the peptide moved well below the membrane head groups. This will be discussed in detail in the next section. Parts a and b of Figure 2 show snapshots of the longest simulation at $t = 0$ ns and $t = 780$ ns, respectively.

Distance between Several System Components and the Middle of the Bilayer. From the masses and positions of all elements of the system, the COM of each component (residues or lipid subgroups) can be calculated. This allowed us to quantify how the peptide approached the membrane surface. Figure 3a shows the time development of the distance of several components from the bilayer's center. This figure corresponds to simulation #2 (Table 1) and shows that, in this particular simulation, the peptide approaches the bilayer from the N-terminus (GLY1). It takes approximately 300 ns for the other end of the peptide, i.e., the LEU27 residue, to completely associate with the bilayer's surface such that the whole peptide is internalized.

A similar analysis, presented in Figure 3b, was carried out for the next longest simulation (#3). The peptide approaches from the C-terminus (LEU27), but despite that, the N-terminus had a higher tendency to go into the bilayer core. In this case, it took ~200 ns for the peptide to completely associate with the bilayer.

In half of the simulations, transportan approached the bilayer surface from the N-terminus (GLY1). In the others, it approached from the C-terminus (LEU27). No matter which end touched the bilayer surface first, the N-terminus of the peptide easily penetrated into the bilayer, while the other end penetrated in a slower fashion. The exception was simulation #1 where the whole peptide associated with the bilayer weakly and no penetration was observed (see also Table 1). In all simulations, it took less than 10 ns for the peptide to reach the membrane's nitrogen atoms.

As is evident from Figure 3a, after $t \sim 600$ ns, the peptide reaches a steady-state position underneath the bilayer head groups. After this time, the distance between the α-carbon atoms of each residue and the bilayer center was measured. The result is shown in Figure 4. Almost 14 α-carbon atoms are below the carbonyl groups of the lipids which are located ~1.5 nm away from the bilayer center. In other words, more than 50% of the peptide penetrated into the hydrophobic region of the bilayer, among which threonine (THR3) and leucine (LEU4) penetrated the most.

The Importance of Lysine Residues. Experiments have shown that the lysine residues in peptides slow down and modulate the penetration process through electrostatic interactions with the bilayer.[3,49,50] To study the importance of lysine residues, we plotted the minimum distance between the NH_3^+ of the four positively charged transportan residues (lysine) and phosphate groups. After 100 ns, all the lysine residues were associated with the phosphate groups and maintained a minimum distance of less than 0.2 nm throughout the simulation. This is partly because of the electrostatic interaction between the positively charged side chains and the bilayer's negatively charged phosphate groups. The other reason, as indicated by Figure 5, is the hydrogen bonding between these residues and the membrane head groups. As shown in the figure, these side chains always maintain at least one hydrogen bond with the phosphate groups. Further

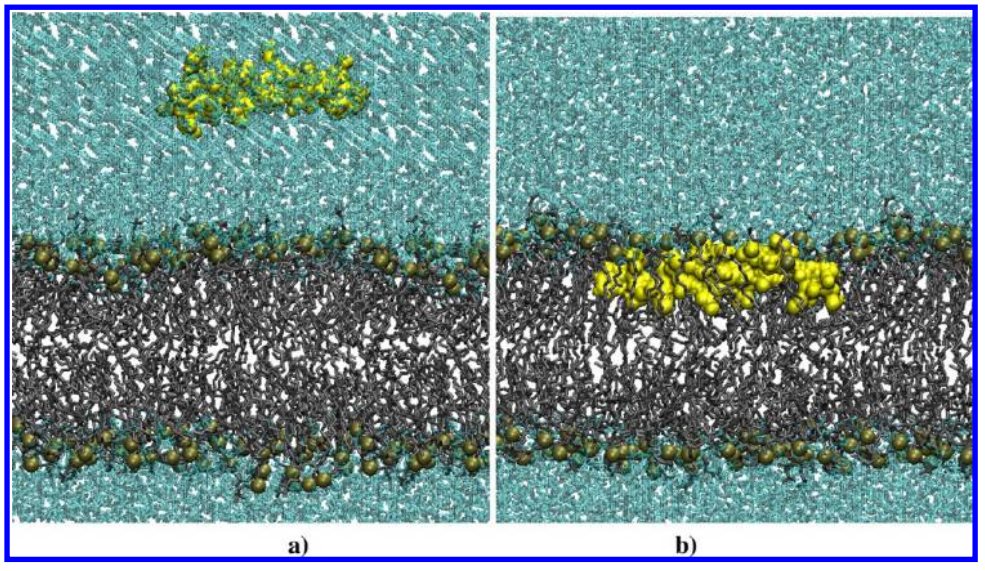

Figure 2. Snapshots of the longest simulation at (a) $t = 0$ ns and (b) $t = 780$ ns. The peptide is shown in *yellow*, the lipids in *gray*, and the water molecules in *blue*.

dx.doi.org/10.1021/jp310255r | J. Phys. Chem. B 2013, 117, 230–241

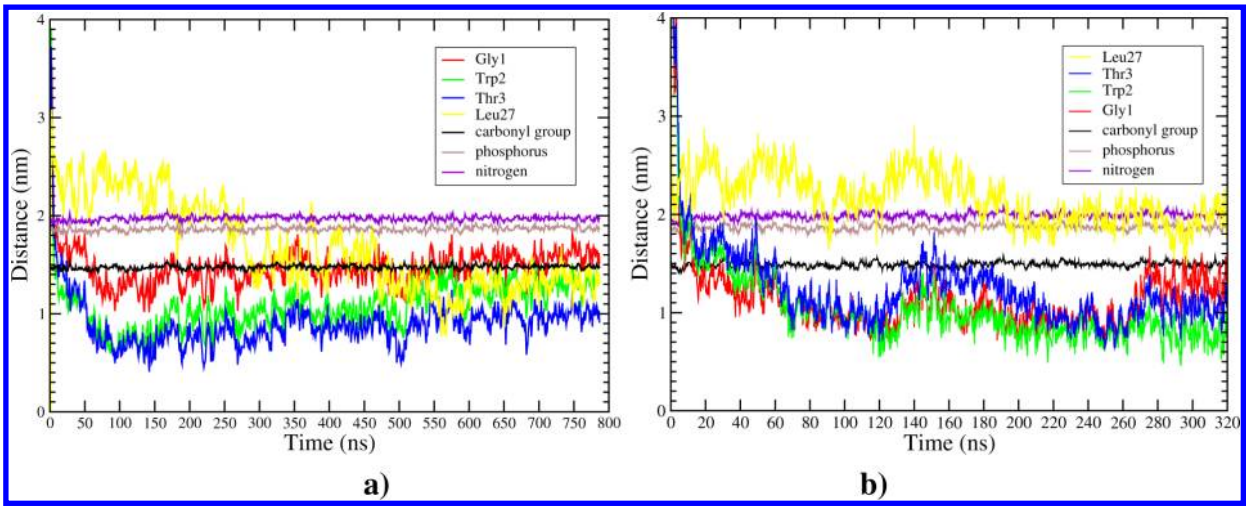

Figure 3. Vertical distance (along the *z*-axis) of several components of the system from the middle of the bilayer obtained from (a) simulation #2 and (b) simulation #3. The bilayer normal is along the *z*-axis, and the *z*-coordinate of the center of mass of the whole bilayer is set to zero. Color coding: *yellow* (LEU27), *blue* (THR3), *green* (TRP2), *red* (GLY1), *black* (carbonyl groups of lipids), *brown* (phosphorus atoms of lipids), and *violet* (nitrogen atoms of lipids).

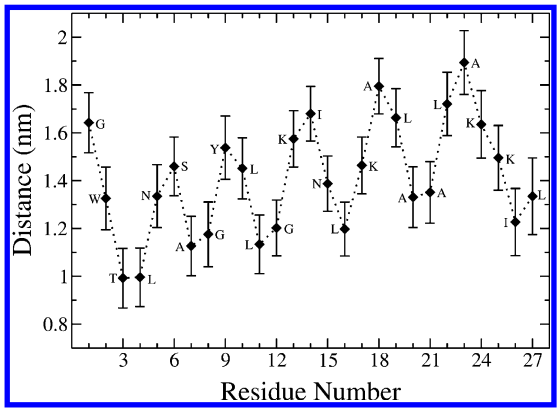

Figure 4. Average distance between α-carbon atoms of each residue and the COM of the bilayer. Averages were taken from t = 600 ns to t = 780 ns of simulation #2.

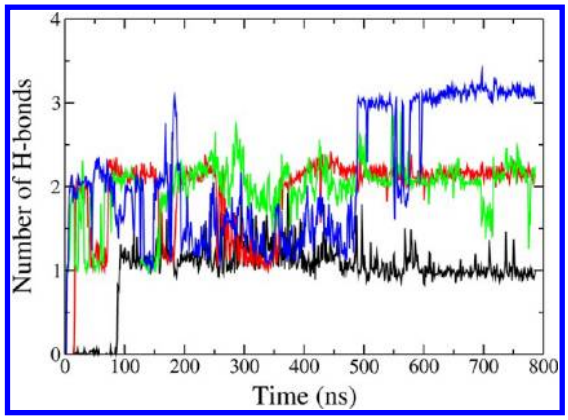

Figure 5. Number of hydrogen bonds between LYS13, LYS17, LYS24, and LYS25 with lipid phosphate groups. Color coding: *black* (LYS13), *red* (LYS14), *green* (LYS24), and *blue* (LYS25).

analyses showed that the main contribution to the hydrogen bonds comes from the NH_3^+ of the lysine's side chains rather than from the NH groups of these residues.

The analyses in this section show how tightly lysine residues are bonded with the membrane. This is in line with the result obtained by Lee et al.[17] who studied the interaction of POPC membranes and Tp10, the shorter version of transportan consisting of 16 amino acids. They showed that the lysine–phosphate interaction is very important in peptide orientation as well as the peptide–membrane interaction.

Area per Lipid and Thickness. The area per lipid is defined as the surface area divided by the number of molecules per leaflet and is experimentally accessible by NMR. In a single component PC bilayer, the average area per PC is calculated simply by dividing the total cross-sectional area by the number of PCs in one monolayer. In our system, the bilayer had an associated transportan, but for consistency, we computed the area per lipid the same way to see the effect of transportan. The average values of the area per DPPC were found to be 0.66 ± 0.01 and 0.65 ± 0.01 nm^2 for DPPC–transportan and pure DPPC systems, respectively; there is no change in area per lipid within measurement accuracy. The value obtained for the pure DPPC system is in perfect agreement with other simulations and experiments.[51,52]

Membrane thickness is not a uniquely defined parameter, and several definitions exist. Since we are interested in the comparison of the thickness of the pure bilayer and the one associated with the peptide, we defined the thickness as the distance between the nitrogen atoms of the two monolayers. The thicknesses of peptide's neighboring and distant lipids were found to be 3.84 ± 0.14 and 3.93 ± 0.08 nm, respectively. In pure DPPC, the average thickness was found to be 3.86 ± 0.04 nm. For all of these values, the error bars overlap and no clear change can be attributed to the bilayer due to the presence of transportan. This is consistent with the fact that there was no change in the area per lipid. We also measured the average value of the minimum thickness of the bilayer to see how much membrane thinning could happen. The values of minimum thickness in transportan–DPPC and pure DPPC systems were found to be 2.54 ± 0.17 and 2.70 ± 0.16 nm, respectively. This shows a 6% decrease in the membrane minimum thickness when it is interacting with transportan compared to the case of a free membrane.

Order Parameter. Robinson et al.[53] were the first to show the ordering effect in MD simulations. To quantitatively

dx.doi.org/10.1021/jp310255r | J. Phys. Chem. B 2013, 117, 230–241

evaluate the order of lipid chains, we use the molecular order parameter

$$S_{mol} = \frac{1}{2}\langle 3\cos^2(\theta_n) - 1\rangle$$

where θ_n is the instantaneous angle between the bilayer normal and the nth segmental vector, i.e., (C_{n-1}, C_{n+1}), the vector linking $n-1$ and $n+1$ carbon atoms in the hydrocarbon chain. The angular brackets, $\langle\cdots\rangle$, denote both the ensemble and the time averages. S_{mol} is closely related to the deuterium order parameter (S_{cd}) and is measured in NMR spectroscopy: $S_{mol} = -2S_{cd}$[54,55] which holds for saturated chains.

Figure 6 shows the order parameter of neighboring and distant lipids, as well as the one for pure DPPC, calculated for the carbon atoms of *sn*-2 acyl chains. The order parameter obtained for pure DPPC is in excellent agreement with previous studies.[48,56] A significant increase in ordering of the upper carbons of lipid tails can be observed due to the presence of transportan. This behavior is different from penetratin–POPC systems: Lensink et al.[24] showed that the presence of penetratin introduces disorder over the entire length of the lipids. Moreover, MD simulation of melittin, an AMP, shows that lipid molecules associated with the peptide are less ordered while those further away are more ordered.[25,57] In the case of transportan, we see a rather different behavior: Local C_{17}, C_{18}, C_{19}, and C_{20} are more ordered than nonlocal ones. Electrostatic interactions between the peptide and head groups of local lipids constrain the carbon atoms that are close enough to head groups, leading to a higher order parameter than the average.

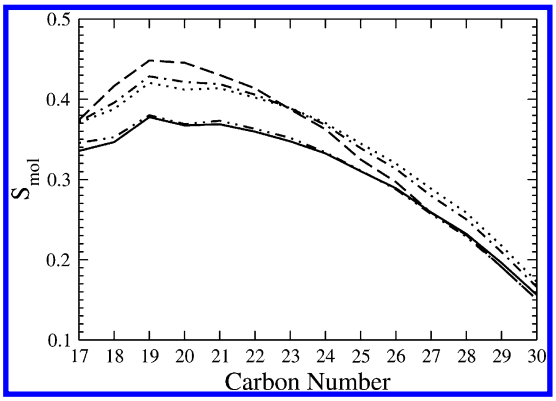

Figure 6. Order parameter, S_{mol}, of the *sn*-2 chain of lipids in the pure DPPC system (*solid line*), lipids not more than 0.6 nm away from the peptide (*dashed line*), lipids more than 0.6 nm away from the peptide (*dotted line*), averaged over the monolayer that contains the peptide (*dashed-dotted*), and averaged over the monolayer that does not contain the peptide (*dashed-double-dotted*) obtained from t = 600 ns to t = 780 ns.

In Figure 7, the order parameters of the lipids in the associated (the peptide is in the large white area) and free monolayers are shown as contour maps in which each color shows regions with the same value of order parameter. The average order parameter of the C_{19} carbon atom of *sn*-2 acyl chains was computed from t = 710 ns to t = 715 ns. This time interval provides enough statistics for averages, and is still short enough for computing the nearly instant order parameter at $t \sim$ 710 ns. At this time, the system is in equilibrium and its properties, such as the conformation of the peptide, remain unchanged (cf. the section Peptide Conformation). A comparison of parts a and b of Figure 7 shows another justification for the fact that neighboring lipids of the peptide, and in general the associated monolayer, are more ordered. Figure 8 shows a snapshot of two neighboring lipids of the peptide and their ordered orientation.

P–N Angle. Using the positions of the phosphorus and nitrogen atoms (Figure 1a), one can calculate the angle between the bilayer normal and the vector linking those atoms in each lipid. The angle distribution of the P–N vector around the z-axis, corresponding to 600–780 ns of the longest simulation, is shown in Figure 9. For the case of pure DPPC, the distribution is in excellent agreement with previous studies.[56] In general, the P–N vector has a tendency to be in the bilayer plane (θ = 90°). However, this tendency is influenced by the presence of transportan. P–N vectors of neighboring lipids make smaller angles with the bilayer normal than P–N vectors of distant lipids. This leads to an ordering of the lipids' head groups and is consistent with the ordered behavior of carbons close to the head groups (cf. Figure 6). The mean values of the P–N angle of pure DPPC lipids, neighboring lipids, distant lipids, and lipids of the unperturbed monolayer are 79.3 ± 0.2, 73.0 ± 0.2, 77.8 ± 0.2, and 79.1 ±

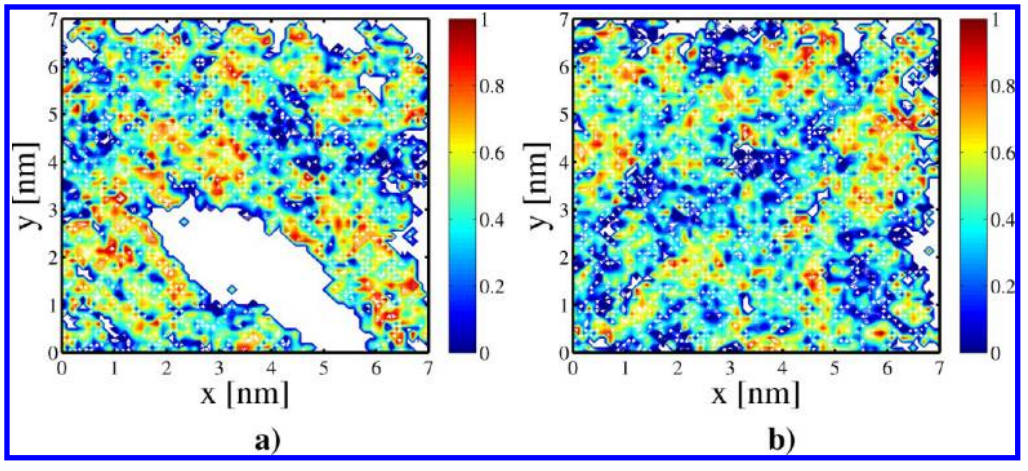

Figure 7. The contour maps of the order parameter of C_{19} of *sn*-2 chains, which has the maximum value of order parameter in Figure 6, in (a) the monolayer that contains the peptide, (b) and the monolayer that does not contain the peptide, averaged from t = 710 ns to t = 715 ns. In (a), the position of the peptide is shown as the white region.

dx.doi.org/10.1021/jp310255r | J. Phys. Chem. B 2013, 117, 230–241

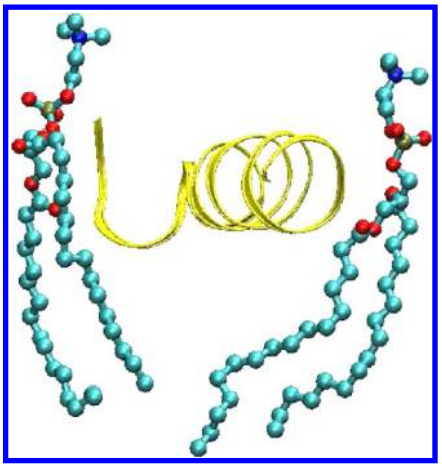

Figure 8. A snapshot of two neighboring lipids of the peptide. The lipids' head groups as well as carbon atoms close to head groups are more ordered compared to distant lipids.

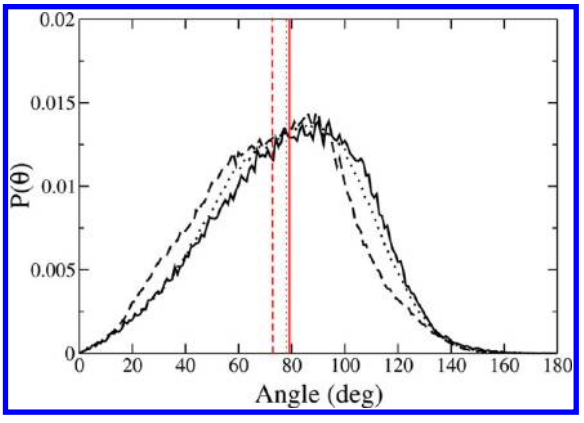

Figure 9. The distribution of the angle between the P−N vector and the bilayer normal (*z*-axis) for lipids in the pure DPPC system (*solid line*), for lipids not more than 0.6 nm away from the peptide in the peptide-associated monolayer (*dashed line*), and for lipids more than 0.6 nm away from the peptide in the peptide-associated monolayer (*dotted line*). The mean values are shown in *red* with the same line style.

0.2°, respectively. The P−N angles of the pure DPPC lipids and the lipids of unperturbed monolayer are within error bars. In the perturbed monolayer, the ordering of the lipids' head groups dies off by 3.3 nm away from the peptide. Farther lipids have a P−N angle closer to that of unperturbed lipids.

In Figure 10, the P−N angle of the lipids in the associated and free monolayers is shown as contour maps. The average P−N angle was computed from t = 700 ns to t = 705 ns, and each color shows regions with the same P−N angle. A comparison of parts a and b of Figure 10 shows a distinct ordering of the lipid head groups that are neighboring the peptide. This is also evident from Figure 8, which shows a snapshot of two neighboring lipids.

Water Defect. A water defect is the penetration of water molecules into the bilayer hydrophobic core. When a part of the peptide is inside the bilayer, water molecules can diffuse into the bilayer interior to solvate the hydrophilic parts of the peptide. Water defects can facilitate peptide penetration and may lead to formation of pores. It has been found that ions can diffuse across the bilayer in a water-defect-mediated fashion without the lipid head groups redistributing themselves to make a pore, although in certain cases it can be pore-mediated.[58] Our analysis showed that at least one water molecule resided in the bilayer core at most of the times. Water defects did not lead to any pore formation in our simulations.

Peptide Conformation. At $t \sim 600$ ns in the longest simulation, up to the sixth residue counted from the N-terminus, the peptide adopted a turn conformation. From the 7th to the 12th residue, it took an α-helix conformation, and from the 13th to the 23rd residue, it was found to be a 5-helix conformation. The rest of the peptide had a coil conformation. The secondary structure of the peptide remained unchanged for the rest of the simulation. Consistent with experiments,[22] the peptide adopted a mostly helical conformation when associated with the bilayer.

The change in the peptide's conformation at $t \sim 600$ ns correlates with the sudden change in the number of hydrogen bonds between LYS25 and the membrane surface, as shown in Figure 5, another sign of the importance of lysine residues.

Equilibrium Simulations 2: Transportan Inserted into the Bilayer. To study the behavior of transportan inside the bilayer core, we performed four simulations up to 172 ns.

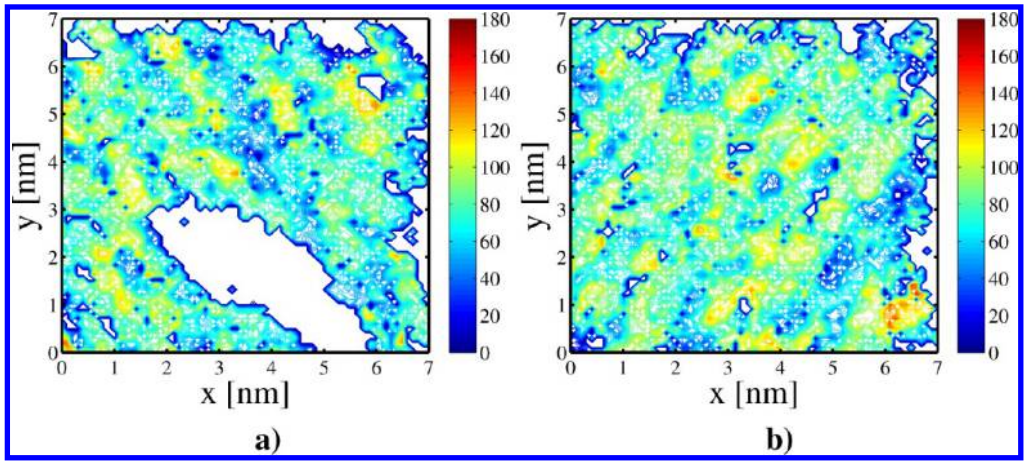

Figure 10. The contour maps of the P−N angle of lipids in (a) the monolayer that contains the peptide and (b) the monolayer that does not contain the peptide. The P−N angles were obtained by averaging from t = 710 ns to t = 715 ns. In (a), the position of the peptide is apparent as a white region where lipids cannot have access. The lower the angle, the more ordered the lipids.

dx.doi.org/10.1021/jp310255r | J. Phys. Chem. B 2013, 117, 230−241

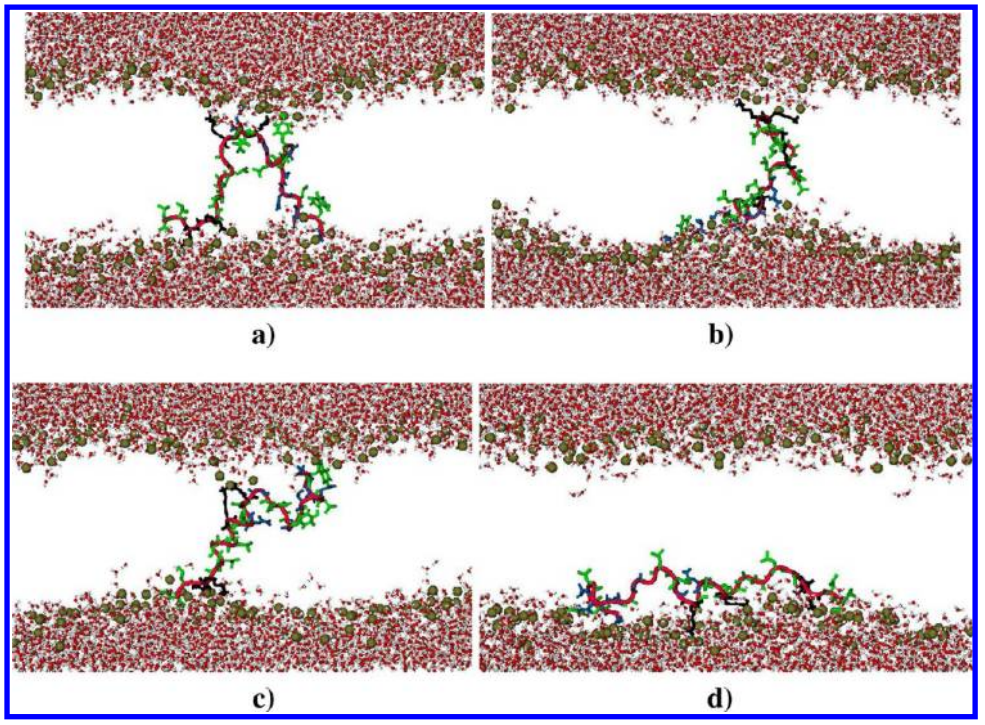

Figure 11. Transportan was inserted horizontally into the bilayer's center: (a) last configuration of simulation #1 after 172 ns, (b) last configuration of simulation #2 after 172 ns, (c) last configuration of simulation #3 after 164 ns, and (d) last configuration of simulation #4 after 134 ns. Phosphorus atoms are shown as balls in *tan*, lysine residues in *black*, hydrophilic residues in *blue*, and hydrophobic residues in *green*. The overall conformation of the peptide is shown as a tube in *red*.

These simulations are complementary to simulations of the previous section in which the peptide initially started from the water phase. For the initial configurations, the peptide was placed horizontally (parallel to the bilayer surface) into the bilayer core. Figure 11 shows the last configurations of these simulations; the initial configuration was parallel to the membrane plane at the center of the bilayer. In other simulations, the initial configuration of the peptide was obtained by rotating it around its axis by a random angle.

The Importance of Lysine, Glycine, and Lucine Residues. Immediately after beginning the inserted-transportan simulations, the peptide was attracted to the phosphate groups of the bilayer's surface via lysine and glycine (GLY1). As shown in Figure 11, in three of the simulations, the peptide bent itself inside the bilayer core. In all of these three cases, bending occurred at the position of a leucine residue. In simulation #1, the peptide bent at LEU11 and LEU16, in simulation #2, it bent at LEU19 and LEU22, and in simulation #3, it bent at LEU10 and LEU11. Therefore, lysine, glycine, and leucine residues play an important role in the peptide conformation inside the bilayer.

The Area per Lipid and Thickness. Similarly to the above simulations, the area per lipid and thickness of the bilayer were computed. The results are presented in Table 2. Comparing the thickness values of the simulations where the peptide was initially in the water phase and Table 2, one can see that the insertion of transportan affects the membrane thickness and causes the bilayer to thin. The comparison shows that the average thickness increases or remains unchanged within the error bars. However, the minimum thickness of the bilayer can decrease by 20% compared to the case where transportan started from water, and by 25% compared to the pure DPPC system. Membrane thinning has been proposed to be a critical determinant of membrane perturbation and pore formation.[59]

Table 2. Area per Lipid, Average Thickness, and Minimum Thickness of the Bilayer When Transportan Is Directly Inserted into the Bilayer's Core

number	simulation length (ns)	area per lipid (nm^2)	average thickness (nm)	minimum thickness (nm)
1	172	0.64 ± 0.01	3.97 ± 0.05	2.56 ± 0.13
2	172	0.65 ± 0.01	3.93 ± 0.04	2.03 ± 0.07
3	164	0.66 ± 0.01	3.93 ± 0.05	2.09 ± 0.13
4	134	0.65 ± 0.01	3.93 ± 0.05	2.58 ± 0.15

Water Defect. We computed the 2D number-density maps of water and phosphate groups to determine how much water has crossed the water−membrane interface, which is defined by the position of phosphate groups. Water molecules are able to penetrate into the bilayer core to keep the phosphate groups as well as the hydrophilic residues of the peptide solvated. We will return to this issue in connection with umbrella sampling below.

Order Parameter. To see if the presence of transportan inside the bilayer core destabilizes the membrane, we computed the order parameter for the *sn*-2 acyl chain of DPPC lipids. The results are presented in Figure 12. Interestingly, in most of the carbon atoms (C_{21} to C_{30}), the order parameter is higher for transportan−DPPC systems compared to a pure DPPC system. On the other hand, in the normal simulations, with the peptide associated to the bilayer's surface but not completely inside the bilayer core, the order parameter for carbon atoms close to head groups (C_{17} to C_{20}) was higher for transportan−DPPC systems compared to pure DPPC (cf. Figure 6). On the basis of these observations, we can conclude that, wherever transportan is inside a bilayer, it induces order in its neighboring lipids.

dx.doi.org/10.1021/jp310255r | J. Phys. Chem. B 2013, 117, 230−241

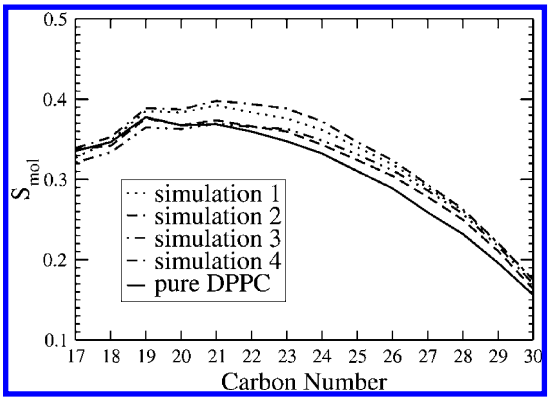

Figure 12. Order parameter, S_{mol}, of *sn*-2 acyl chains of DPPC in the inserted-transportan simulations obtained from the last 30 ns of the simulations. See Figure 11 and Table 2 for more information and the numbering of simulations.

Simulations 3: Free Energy Calculations. We used umbrella sampling to compute the Gibbs free energy of the system when the peptide is at different distances from the center of the bilayer. The free energy profile along the *z*-axis shown in Figures 13 and 14 shows snapshots from the

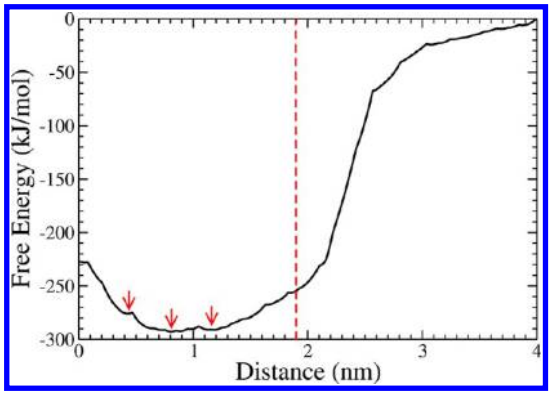

Figure 13. Free energy as a function of the peptide's distance from the bilayer's center. The bilayer's center is set to zero. The water–membrane interface, defined as the average position of phosphorus atoms in the unbiased simulations, is shown as a *dashed line* in *red*. There are three important energy minima at z = 0.4 nm, z = 0.8 nm,and z = 1.2 nm, as indicated by the arrows.

simulation. The free energy is higher when the peptide is in the water than when it is inside the bilayer. This shows the tendency of the peptide for passive translocation. However, going from one monolayer to the other, the peptide must overcome the possible energy barriers between the two leaflets. The first smaller bump is located between 1.0 and 1.1 nm from the bilayer's center, the next one is around 0.5 nm from the bilayer's center, and the last one is in the middle of the bilayer.

There are three shallow minima corresponding to the bumps: one around 0.4 nm, one around 0.8 nm, and the other around 1.2 nm from the bilayer's center. When the peptide is around 1.2 nm from the bilayer's center, it is highly associated with the bilayer's surface. Figure 14d shows a snapshot of the peptide at this position. When it is around 0.8 nm from the bilayer's center, some of its hydrophobic residues have freed themselves from the bilayer's hydrophilic center (Figure 14c). When it is around 0.4 nm from the bilayer's center, the lysine residue LYS25 frees itself from one monolayer and is attracted to the other one (Figure 14b). This is where crossing from one monolayer to the other occurs. In regions with z > 0.4 nm, the peptide is associated with only one monolayer. In regions between z = 0 nm and z = 0.4 nm, the peptide is associated with both monolayers. Interestingly, Mark et al. found a similar local minimum ~0.4 nm in the free energy profile of penetratin interacting with a DPPC bilayer.[12] Unlike penetratin for which the crossing from the interfacial region to the central region is associated with the formation of a toroidal-like pore, no pore formation was induced by transportan.

To complete translocation, all remaining residues should free themselves, and to accomplish this, they should pass a potential barrier located in the middle of the bilayer (Figure 14a). This is the main potential barrier in the free energy profile, and its height is approximately 66 kJ/mol when measured as the difference between the absolute free energy minimum and the free energy in the bilayer center. According to the Eyring theory,[60,61] this barrier is in principle accessible at 323 K on time scales of milliseconds, i.e., $\tau = (h/kT)e^{\Delta G/kT}$ = 0.007 s, where h is the Planck constant. The height of this barrier is less than the barrier corresponding to the flip-flop of a single DPPC lipid which is ~80 kJ/mol.[62] As another comparison, the potential barrier for penetratin translocation through DPPC lipids is ~75 kJ/mol.[12]

Figure 15 shows the water defect when the peptide is restrained at z = 0 nm and z = 0.4 nm. When the peptide is restrained at z = 0.4 nm, the water defect is more noticeable compared to other cases. The insets in Figure 15b and d show snapshots of the system at t = 95 ns (z = 0 nm) and t = 81 ns (z = 0.4 nm), respectively. The water defect in the later case is noticeable.

Peptide Helicity. Figure 16 shows the α-helicity of the peptide as it is restrained at different positions along the *z*-axis. The α-helicity is the highest (~60%) when the peptide is ~0.4 nm from the bilayer center. At this distance, the system has a local minimum of the free energy (cf. Figure 13). There is also a jump in the α-helicity of the peptide when it is restrained at z = 0.8 nm, which corresponds to another minimum of free energy. The region where the peptide has almost the same α-helicity is between z = 1.1 nm and z = 1.6 nm, i.e., close to lipids' carbonyl groups. See Figure 14 for the snapshots of the peptide at these locations.

Let us speculate on the penetration mechanism now. As outlined in the Introduction, there are several mechanisms involved in the action of AMPs and CPPs. Almeida et al. hypothesized that the thermodynamics as well as kinetics of insertion of peptides, rather than their sequences, determine their behavior.[3] In their hypothesis, the difference between the free energy when the peptide is at the water–membrane interface, $G_{interface}$, and when it is completely inserted into the bilayer core, $G_{inserted}$, is important. If $\Delta G = G_{inserted} - G_{interface}$ is greater than ~84 kJ/mol, the partitioning of the peptide in the bilayer is very unfavorable. In this case, peptides follow the "all-or-none" mechanism. They accumulate at the water–membrane interface until a pore forms in the bilayer due to peptide-induced defects in the membrane. The peptides then stabilize the pore. *In vitro* experiments use vesicles, and the formation of a stable pore means the release of the contents of the vesicle. In the "graded" mechanism, ΔG is less than ~84 kJ/mol. After accumulation of peptides on the membrane surface, they cross the bilayer to neutralize the mass imbalance across it. Transportan-10, a peptide which lacks the first six residues of transportan from the N-terminus, has been found to follow a

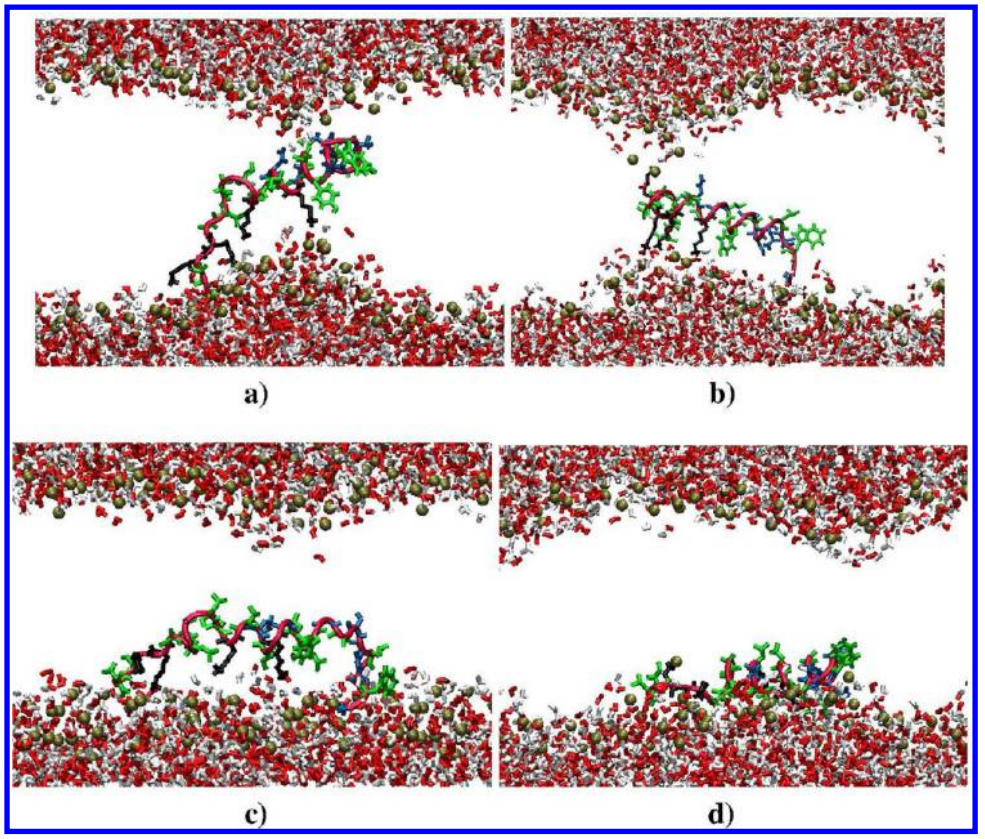

Figure 14. Snapshots of the biased simulations when the peptide is (a) restrained in the middle of the bilayer, (b) 0.4 nm away from the bilayer's center, (c) 0.8 nm away from the bilayer's center, and (d) 1.2 nm away from the bilayer's center. Phosphorus atoms are shown as balls in *tan*, lysine residues in *black*, hydrophilic residues in *blue*, and hydrophobic residues in *green*. The overall conformation of the peptide is shown as a tube in *red*.

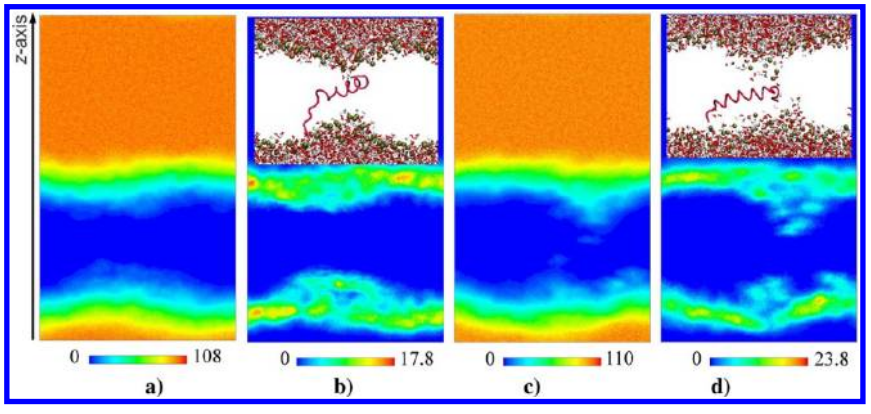

Figure 15. Two-dimensional density map of water ((a) and (c)) and phosphate group (PO_4^{-1}) ((b) and (d)). In (a) and (b), the peptide is restrained at z = 0 nm, and in (c) and (d), the peptide is restrained at z = 0.4 nm. The unit is nm^{-3}, and the vertical axis is along the bilayer normal. The insets in (b) and (d) show snapshots of the system at t = 95 ns and t = 81 ns in which the peptide is restrained at z = 0 nm and z = 0.4 nm, respectively. The water defect in the latter case is noticeable. The peptide is shown in *red*, phosphorus atoms are shown as balls in *tan*, and water molecules are shown in *white-red*.

graded mechanism.[9] That is, accumulation of these peptides strains the membrane. The membrane then lets the peptides in to relieve the strain.

On the basis of the current results, translocation of transportan follows the same mechanism as that of transportan-10. In our study, $\Delta G \sim 65$ kJ/mol, which puts the penetration mechanism of transportan in the graded category. Another sign of such a mechanism is the favorable state of transportan inside the bilayer. What can be proposed from our study is that the peptide reaches the other monolayer through a stochastic process. We have shown here that lysine residues play a significant role in anchoring the peptide to the other monolayer. Moreover, in such a process, water defects can facilitate the sinking of the peptide in the bilayer. On the basis of this, one should expect a slower translocation in the case of shorter analogues of transportan such as transportan-10, because the opposite monolayer is hardly accessible by a shorter peptide. Indeed, it has been found that the penetration of shorter analogues of transportan is slower than that of transportan itself.[18]

dx.doi.org/10.1021/jp310255r | J. Phys. Chem. B 2013, 117, 230−241

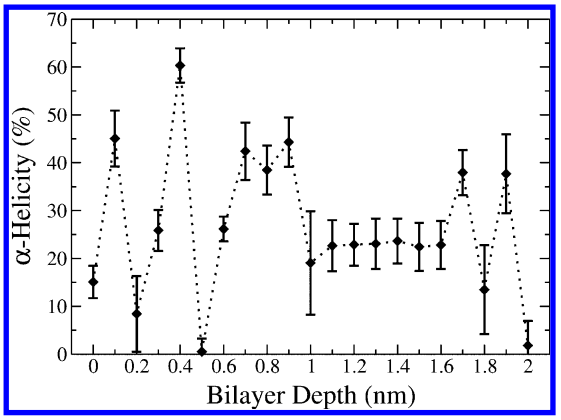

Figure 16. The percentage of α-helicity of the peptide as a function of its distance from the bilayer center.

CONCLUSION

In conclusion, it is energetically favorable for transportan to reside inside the bilayer. At such a state, the neighboring lipids are more ordered than the distant ones. The peptide tries to reach the other monolayer stochastically through the lysine residues, and water defects can facilitate this process. If a connection is made between the two monolayers through the peptide, the bilayer thins significantly and the formation of a pore, either transiently or permanently, is likely to happen.

AUTHOR INFORMATION

Corresponding Author

*E-mail: mikko.karttunen@uwaterloo.ca.

Notes

The authors declare no competing financial interest.

ACKNOWLEDGMENTS

This work was supported in part by the Natural Sciences and Engineering Research Council of Canada (NSERC) (M.K.), the Ontario Early Researcher Award Program (M.K.), the Thailand Research Fund (TRF) (J.W.), Kasetsart University Research and Development Institute (KURDI) (J.W.), and the Faculty of Science at Kasetsart University (J.W.). Computational resources were provided by SharcNet (www.sharcnet.ca).

REFERENCES

(1) Zorko, M.; Langel, Ü. *Adv. Drug Delivery Rev.* **2005**, *57*, 529−545.
(2) El-Andaloussi, E.; Holm, T.; Langel, Ü. *Curr. Pharm. Des.* **2005**, *11*, 529−545.
(3) Almeida, P. F.; Pokorny, A. *Biochemistry* **2009**, *48*, 8083−8093.
(4) Vivès, E.; Richard, J. P.; Rispal, C.; Lebleu, B. *Curr. Protein Pept. Sci.* **2003**, *4*, 13−20.
(5) Leifert, J. A.; Whitton, J. L. *Mol. Ther.* **2003**, *8*, 13−20.
(6) Taylor, C. T.; Furuta, G. T.; Synnestvedt, K.; Colgan, S. P. *Proc. Natl. Acad. Sci. U.S.A.* **2000**, *97*, 12091−12096.
(7) Ehrenstein, G.; Lehar, H. *Q. Rev. Biophys.* **1977**, *10*, 1−34.
(8) Matsuzaki, K.; Murase, O.; Fujii, N.; Miyajima, K. *Biochemistry* **1996**, *35*, 11361−11368.
(9) Yandek, L. E.; Pokorny, A.; Florén, A.; Knoelke, K.; Langel, Ü.; Almeida, P. F. *Biophys. J.* **2007**, *92*, 2434−2444.
(10) Derossi, D.; Calvet, S.; Trembleau, A.; Brunissen, A.; Chassaing, G.; Prochiantz, A. *J. Biol. Chem.* **1996**, *271*, 18188−18193.
(11) Drin, G.; Cottin, S.; Blanc, E.; Rees, A. R.; Temsamani, J. *J. Biol. Chem.* **2003**, *278*, 31192−31201.
(12) Yesylevskyy, S.; Marrink, S. J.; Mark, A. E. *Biophys. J.* **2009**, *97*, 40−49.
(13) Schwarze, S. R.; Hruska, K. A.; Dowdy, S. F. *Trends. Cell Biol.* **2000**, *10*, 290−295.
(14) Langel, Ü.; Pooga, M.; Kairane, C.; Zilmer, M.; Bartfai, T. *Regul. Pept.* **1996**, *62*, 47−52.
(15) Land, T.; Langel, O.; Löw, M.; Berthold, M.; Undén, A.; Bartfai, T. *Int. J. Pept. Protein Res.* **1991**, *38*, 267−272.
(16) Higashijima, T.; S., U.; Nakajima, T.; Ross, E. M. *J. Biol. Chem.* **1988**, *263*, 6491−6494.
(17) Dunkin, C. M.; Pokorny, A.; Almeida, P. F.; Lee, H. S. *J. Phys. Chem. B* **2011**, *115*, 1188−1198.
(18) Soomets, U.; Lindgren, M.; Gallet, X.; Hällbrink, M.; Elmquist, A.; Balaspiri, L.; Zorko, M.; Pooga, M.; Brasseur, R.; Langel, Ü. *Biochim. Biophys. Acta* **2000**, *1467*, 165−176.
(19) Barany-Wallje, E.; Andersson, A.; Gräslund, A.; Maler, L. *FEBS Lett.* **2004**, *567*, 265−269.
(20) Barany-Wallje, E.; Andersson, A.; Gräslund, A.; Maler, L. *J. Biomol. NMR* **2006**, *35*, 137−147.
(21) Pooga, M.; Hallbrink, M.; Zorko, M.; Langel, Ü. *FASEB J.* **1998**, *12*, 67−77.
(22) Lindberg, M.; Jarvet, J.; Langel, Ü.; Gräslund, A. *Biochemistry* **2001**, *40*, 3141−3149.
(23) Chugh, A.; Eudes, F. *J. Pept. Sci.* **2008**, *14*, 477−481.
(24) Lensink, M. F.; Christiaens, B.; Vandekerckhove., J.; Prochiantz, A.; M., R. *Biophys. J.* **2005**, *88*, 939−952.
(25) Sengupta, D.; Leontiadou, H.; Mark, A. E.; Marrink, S. J. *Biochim. Biophys. Acta* **2008**, *1778*, 2308−2317.
(26) Leontiadou, H.; Mark, A. E.; Marrink, S. J. *J. Am. Chem. Soc.* **2006**, *128*, 12156−12161.
(27) Herce, H. D.; Garcia, A. E. *Proc. Natl. Acad. Sci. U.S.A.* **2007**, *104*, 20805−20810.
(28) Hess, B.; Kutzner, C.; van der Spoel, D.; Lindahl, E. *J. Chem. Theory Comput.* **2008**, *4*, 435−477.
(29) Patra, M.; Karttunen, M.; Hyvönen, M. T.; Falck, E.; Vattulainen, I. *J. Phys. Chem. B* **2004**, *108*, 4485−4494.
(30) Berger, O.; Edholm, O.; Jahnig, F. *Biophys. J.* **1997**, *72*, 2002−2013.
(31) van Buuren, A. R.; Marrink, S. J.; Berendsen, H. J. C. *J. Phys. Chem.* **1993**, *97*, 9206−9212.
(32) Mark, A. E.; van Helden, S. P.; Smith, P. E.; Janssen, L. H. M.; van Gunsteren, W. F. *J. Am. Chem. Soc.* **1994**, *116*, 6293−6302.
(33) Cino, E.; Choy, W. Y.; Karttunen, M. *J. Chem. Theory Comput.* **2012**, *8*, 2725−2740.
(34) Wong-Ekkabut, J.; Karttunen, M. *J. Chem. Theory Comput.* **2012**, 2905−2911.
(35) Kukol, A. *J. Chem. Theory Comput.* **2009**, *5*, 615−626.
(36) Ulmschneider, J. P.; B., U. M. *J. Chem. Theory Comput.* **2009**, *5*, 1803−1813.
(37) Poger, D.; van Gunsteren, W. F.; Mark, A. E. *J. Comput. Chem.* **2009**, *31*, 1117−1125.
(38) Berendsen, H. J. C.; Postma, J. P. M.; van Gunsteren, W. F.; Hermans, J. In *Intermolecular Forces*; Pullman, B., Ed.; Reidel: Dordrecht, The Netherlands, 1981; p 331.
(39) Berendsen, H. J. C.; Postma, J. P. M.; van Gunsteren, W. F.; DiNola, A.; Haak, J. R. *J. Chem. Phys.* **1984**, *81*, 3684−3690.
(40) Darden, T.; York, D.; Pedersen, L. *J. Chem. Phys.* **1993**, *98*, 10089−10092.
(41) Patra, M.; Karttunen, M.; Hyvönen, M. T.; Falck, E.; Lindqvist, P.; Vattulainen, I. *Biophys. J.* **2003**, *84*, 3636−3645.
(42) Hess, B.; Bekker, H.; Berendsen, H. J. C.; Fraaije, J. G. E. M. *J. Comput. Chem.* **1997**, *18*, 1463−1472.
(43) Torrie, G. M.; Valleau, J. P. *J. Comput. Phys.* **1977**, *23*, 187−199.
(44) Kumar, S.; Bouzida, D.; Swendsen, R. H.; Kollman, P. A.; Rosenberg, J. M. *J. Comput. Chem.* **1992**, *13*, 1011−1021.
(45) Murzyn, K.; Zhao, W.; Karttunen, M.; Róg, T. *Biointerfaces* **2006**, *1*, 98−105.
(46) Guardia, E.; Marti, J.; Garcia-Tarres, L.; Laria, D. *J. Mol. Liq.* **2005**, *117*, 63−67.
(47) Luzar, A.; Chandler, D. *J. Chem. Phys.* **1993**, *98*, 8160−8173.

(48) Kupiainen, M.; Falck, E.; Ollila, S.; Niemelä, P. S.; Gurtovenko, A. A.; Hyvönen, M. T.; Patra, M.; Karttunen, M.; Vattulainen, I. *J. Comput. Theor. Nanosci.* **2005**, *2*, 401−413.
(49) Wender, P. A.; Mitchell, D. J.; Pattabiraman, K.; Pelkey, E. T.; Sterinman, L.; Rothbard, J. B. *Proc. Natl. Acad. Sci. U.S.A.* **2000**, *97*, 13003−13008.
(50) Yang, L.; Gordon, V. D.; Trinkle, D. R.; Schmidt, N. W.; Davis, M. A.; DeVries, C.; Som, A.; Cronan, J. E., Jr.; Tew, G. N.; Wong, G. C. L. *Proc. Natl. Acad. Sci. U.S.A.* **2008**, *105*, 20595−20600.
(51) Lee, B. W.; Faller, R.; Sum, A. K.; Vattulainen, I.; Patra, M.; Karttunen, M. *Fluid Phase Equilib.* **2004**, *225*, 63−68.
(52) Nagle, J. F.; Zhang, R.; Tristram-Nagle, S.; Sun, W.; Petrache, H. I.; Suter, R. M. *Biophys. J.* **1996**, *70*, 1419−1431.
(53) Robinson, A.; Richards, W. G.; Thomas, P. J.; Hann, M. M. *Biophys. J.* **1995**, *68*, 164−170.
(54) Davis, J. H. *Biochim. Biophys. Acta* **1983**, *737*, 117−171.
(55) Douliez, J. P.; Leonard, A.; Dufourc, E. J. *Biophys. J.* **1995**, *68*, 1727−1739.
(56) Patra, M.; Salonen, E.; Terama, E.; Vattulainen, I.; Faller, R.; Lee, B. W.; Holopainen, J.; Karttunen, M. *Biophys. J.* **2006**, *90*, 1121−1135.
(57) Bachar, M.; Becker, O. M. *Biophys. J.* **2000**, *78*, 1359−1375.
(58) Vattulainen, I.; Gurtovenko, A. A. *Biophys. J.* **2007**, *92*, 1878−1890.
(59) Chen, F.-Y.; Lee, M.-T.; Huang, H. W. *Biophys. J.* **2003**, *84*, 3751−3758.
(60) Eyring, H. *J. Chem. Phys.* **1935**, *3*, 107−115.
(61) Evans, M. G.; Polanyi, M. *Trans. Faraday Soc.* **1935**, *31*, 875−894.
(62) Sapay, N.; Bennett, W. F. D.; Tieleman, D. P. *Soft Matter* **2009**, *5*, 3295−3302.